

## Supporting Information

### Gas-Phase Preparation of Azulene (C<sub>10</sub>H<sub>8</sub>) and Naphthalene (C<sub>10</sub>H<sub>8</sub>) via the Reaction of the Resonantly Stabilized Fulvenallenyl (C<sub>7</sub>H<sub>5</sub><sup>•</sup>) and Propargyl (C<sub>3</sub>H<sub>3</sub><sup>•</sup>) Radicals<sup>†</sup>

Wang Li,<sup>a</sup> Jiuzhong Yang,<sup>a</sup> Long Zhao<sup>\*a,b</sup>

<sup>a</sup> National Synchrotron Radiation Laboratory, University of Science and Technology of  
China, Hefei, Anhui 230029, China

<sup>b</sup> School of Nuclear Science and Technology, University of Science and Technology of China,  
Hefei, Anhui 230027, China

David Couch,<sup>c</sup> Myrsini San Marchi,<sup>c</sup> Nils Hansen<sup>\*c</sup>

<sup>c</sup> Combustion Research Facility, Sandia National Laboratories, Livermore, CA 94551, USA

Alexander N. Morozov,<sup>d</sup> Alexander M. Mebel<sup>\*d</sup>

<sup>d</sup> Department of Chemistry and Biochemistry, Florida International University, Miami, FL  
33199, USA

Ralf I. Kaiser<sup>\*e</sup>

<sup>e</sup> Department of Chemistry, University of Hawaii at Manoa, Honolulu, HI 96822, USA

---

<sup>†</sup> Electronic supplementary information (ESI) available: Experimental section (Figs. S1-S3); additional PIE curves (Figs. S4-S8); phthalide pyrolysis (Figs. S9-S11); absolute photoionization cross-section (PICS) of azulene (Fig. S12); fit of PIE at m/z=128 (Figs. S13-S14); computational methods (Section 6); potential energy diagram illustrated with the structures of representative transition states (Fig. S15); product branching ratios (Fig. S16).

\* Corresponding authors: Long Zhao [zhaolong@ustc.edu.cn](mailto:zhaolong@ustc.edu.cn); Nils Hansen [nhansen@sandia.gov](mailto:nhansen@sandia.gov); Alexander M. Mebel [mebel@fiu.edu](mailto:mebel@fiu.edu); Ralf I Kaiser [ralfk@hawaii.edu](mailto:ralfk@hawaii.edu)

## **Supplemental Material**

### **Table of Contents**

**Section 1: Experimental Section**

**Section 2: Additional PIE curves**

**Section 3: Phthalide pyrolysis.**

**Section 4: Absolute photoionization cross-section (PICS) of azulene**

**Section 5: Fit of PIE at  $m/z=128$ .**

**Section 6: Computational methods**

**Section 7: Potential energy diagrams with representative transition states structures**

**Section 8: Product branching ratios**

## Section 1:

### Experimental Section (Electron Ionization Mass Spectrometry - Sandia)

The experimental setup at Sandia has been described previously.<sup>1</sup> It consists of a resistively heated silicon carbide (SiC) tube and an orthogonal extraction mass spectrometer with an electron gun for ionization of the sampled molecules. The silicon carbide tube is 28.0 mm long with an inner diameter of 1.2 mm. About 10.0 mm is heated resistively, with about 3.0 mm at the end that is not heated (Fig. S1). A thermal camera measures the temperature profile of the tube with an accuracy of  $\pm 50$  K for the SiC tube and the carbon disks contacting the tube. The pressure in the hottest part of the reactor is about 30 Torr, based on a prior flow simulation under similar conditions.<sup>2</sup>

We used phthalide ( $C_8H_6O_2$ , Fig. S3a, 98%, Sigma-Aldrich) and propargyl bromide ( $C_3H_3Br$ , Sigma-Aldrich) as precursors for the fulvenallenyl ( $C_7H_5$ ) and propargyl ( $C_3H_3$ ) radicals, respectively. A mixture of  $C_3H_3Br$  in He was prepared in advance, while phthalide was placed in a bubbler with helium flowing across the top of the sample. Parallel mass flow controllers controlled the flow of helium through the phthalide bubbler and the flow of prediluted  $C_3H_3Br$  for a constant total flow rate of 50.0 SCCM (standard cubic centimeter per minute) and a constant 0.2% total concentration of  $C_3H_3Br$ ; higher concentrations must be avoided to eliminate propargyl radical self-reactions. The phthalide bubbler was held in a hot water bath at around 343 K to promote sublimation, and all lines downstream from the bubbler were heated with heat tape to prevent condensation. The flow exiting the reactor creates a supersonic expansion that rapidly cools the molecular beam. This molecular beam is sampled

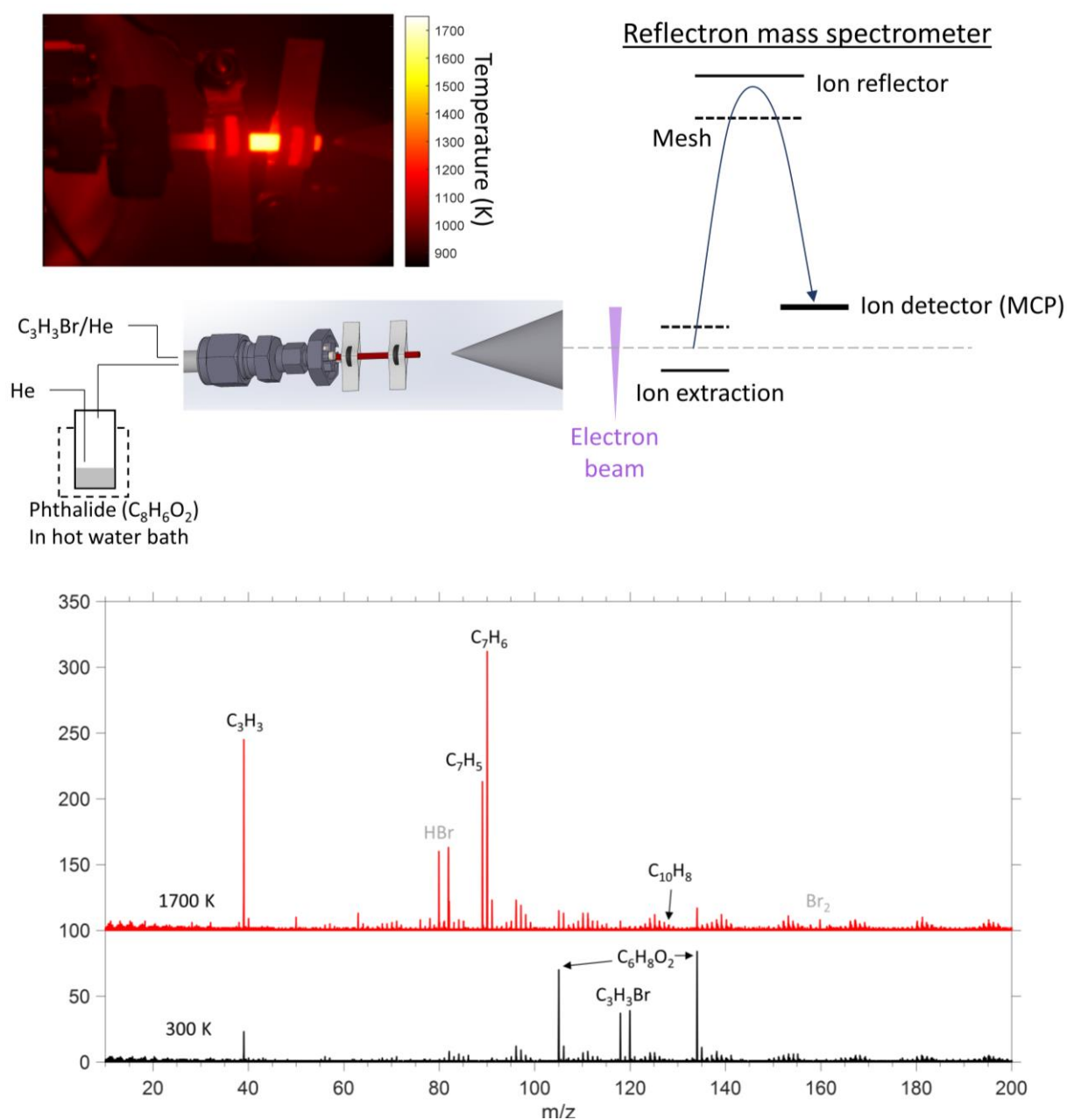


**Fig. S1** Upper part: Experimental setup for Sandia reactor. The thermal camera image shows measured temperature at the hottest conditions used in this work. Lower part: Sample mass spectra at two different reactor temperatures.

by a 0.4 mm diameter nickel skimmer to a high vacuum chamber, where an electron-ionization mass spectrometer characterizes the chemical composition of the beam. For the present experiment, the electron source was tuned to 13 eV (FWHM around 2 eV), which minimizes

the dissociative ionization of  $C_7H_6$  into  $m/z = 89$  while still maintaining a useable total ionization rate. More information about the spectrometer is available.<sup>3,4</sup>

The lower portion of Fig. S1 contains sample mass spectra at two different temperatures.

### **Experimental Section (Photoionization - Hefei)**

The experiments, utilizing a high-temperature chemical reactor (Fig. S2a), were carried out at Combustion Endstation (BL03U) of the National Synchrotron Radiation Laboratory (NSRL) in Hefei, China.<sup>5</sup> The reactor is consisted of a silicon carbide (SiC) tube (40.00 mm long with the heating length of 20.00 mm in the center, 1.00 mm i.d., 2.00 mm o.d.), mounted in a high vacuum chamber ( $\sim 10^{-6}$  Torr). In the present work, the reactive fulvenallenyl ( $C_7H_5^*$ ) and propargyl ( $C_3H_3^*$ ) radicals were generated *in-situ* in the SiC reactor by thermal decomposition of the two precursors, trichloromethyl-benzene ( $C_7H_5Cl_3$ , Fig. S3b, Aladdin, > 99%) and propargyl bromide ( $C_3H_3Br$ , TCL, > 97%), respectively. In details, the two liquid precursors were kept in two separate bubblers at the temperatures of 283 K (thermostatic bath, Hangzhou Qiwei Instrument Co., Ltd) and 199 K (drikold/ethanol bath) (Fig. S2b), with helium (He) carrier gas fed into the bubblers at the flow rates of 20.0 and 10.0 SCCM, respectively, controlled by mass flow controllers (MKS, Andover, MA, USA). The vapors were seeded into He and sufficiently mixed reaching a total pressure of 280 Torr monitored by a PMS pressure sensor (PMS 111, BD Sensor Co., Ltd). The gas mixture passed through a stainless-steel nozzle with a 0.1 mm aperture, forming a continuous supersonic molecular beam before entering the SiC reaction region, which was resistively heated to  $998 \pm 10$  K measured by a Type-S thermocouple. After exiting the reactor, the molecular beam with products was sampled through a 2.0 mm diameter nickel skimmer located 10.0 mm downstream of the pyrolytic

reactor, crossed perpendicularly with the synchrotron tunable vacuum ultraviolet (SVUV) light, fragment-free photoionized and then detected by a reflection time-of-flight mass spectrometer (Re-TOF-MS).<sup>5,6</sup> Photoionization efficiency (PIE) curves ranged from 7.20 to 9.00 eV with a step interval of 0.05 eV were recorded to identify the specific mass-to-charge ratio ( $m/z$ ) for the species of interest. Control experiments were conducted by expanding He carrier gas into the SiC tube with only trichloromethyl-benzene seeded.

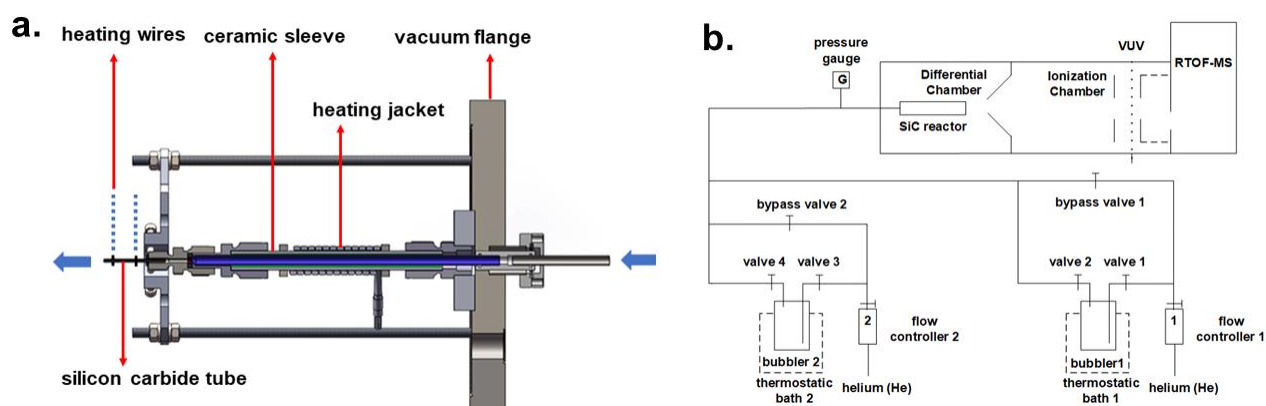


**Fig. S2** Experimental facility in Hefei. (a) Detailed schematic diagram of silicon carbide tubular reactor. (b) Simplified schematic diagram of experimental facility combined with SVUV and RTOF-MS.

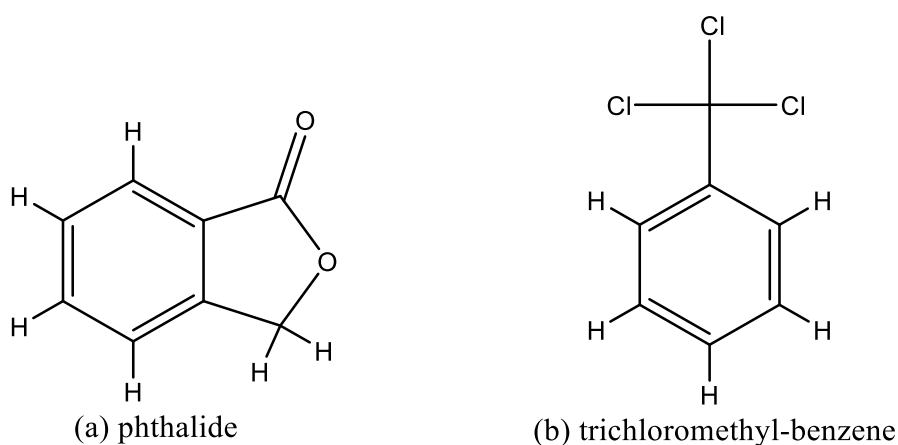


**Fig. S3** Structures of two precursors, phthalide and trichloromethyl-benzene, generating fulvenallenyl in this work.

## Section 2: Additional PIE curves.

Signals ( $m/z=89, 124, 126, 159, 161$  and  $163$ ) in Figs. 2b-2c is related to the stepwise elimination of Cl atom from  $C_7H_5Cl_3$  molecule: a) One Cl atom losing-  $m/z=159$  ( $C_7H_5^{35}Cl_2^+$ ),  $161$  ( $C_7H_5^{35}Cl^{37}Cl^+$ ) and  $163$  ( $C_7H_5^{37}Cl_2^+$ ); b) Two Cl atoms losing-  $m/z=124$  ( $C_7H_5^{35}Cl^+$ ) and  $126$  ( $C_7H_5^{37}Cl^+$ ); c) Cl atoms losing completely-  $m/z=89$  ( $C_7H_5^+$ ). Notably, ion counts at  $m/z=87$  ( $C_7H_3^+$ ),  $88$  ( $^{13}CC_6H_3^+$ ),  $90$  ( $^{13}CC_6H_5^+/C_7H_6^+$ ),  $123$  ( $C_7H_4^{35}Cl^+$ ),  $125$  ( $^{13}CC_6H_5^{35}Cl^+/C_7H_4^{37}Cl^+$ ),  $127$  ( $^{13}CC_6H_5^{37}Cl^+/C_7H_6^{37}Cl^+$ ),  $160$  ( $^{13}CC_6H_5^{37}Cl_2^+/C_7H_4^{35}Cl^{37}Cl^+$ ),  $162$  ( $^{13}CC_6H_5^{35}Cl^{37}Cl^+/C_7H_4^{37}Cl_2^+$ ) and  $164$  ( $^{13}CC_6H_5^{37}Cl_2^+/C_7H_6^{37}Cl_2^+$ ) are detectable in high-temperature experiments (Figs. 2b and 2c). These signals can be connected to H-elimination and/or  $^{13}C$  isotopes of radicals ( $m/z=89, 124, 126, 159, 161$  and  $163$ ) generated from stepwise Cl-loss of  $C_7H_5Cl_3$ .

PIE curves of species produced from Cl-loss of  $C_7H_5Cl_3$  molecule are exhibited in Figs. S4-S6. Figure S4 shows PIE curves of species at  $m/z=87, 88, 90$  and  $91$  connecting with three Cl atoms losing completely from  $C_7H_5Cl_3$  molecule. Accompanied with fulvenallenyl radical, fulvenallene ( $C_7H_6$ ,  $m/z=90$ ) and benzyl ( $C_7H_7^{\bullet}$ ,  $m/z=91$ ) are also formed and determined based on PIE curves (Figs. S4c and S4d), though, the content of both of them are minor. Figures S4a and S4b present PIE curves for species at  $m/z=87$  and  $88$  which could result from stepwise H-elimination from fulvenallenyl under the elevated experimental temperature.

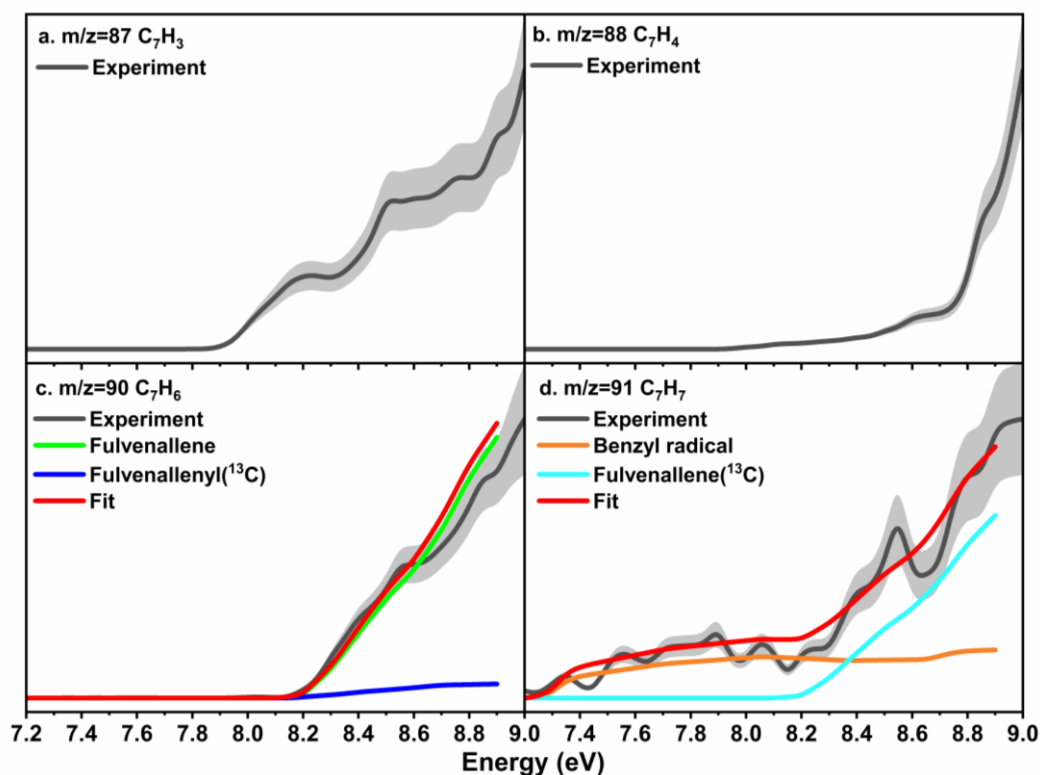


**Fig. S4** Experimental and reference PIE curves for species at  $m/z=87$ ,  $88$ ,  $90$  and  $91$  in trichloromethyl-benzene ( $C_7H_5Cl_3$ )/propargyl bromide ( $C_3H_3Br$ ) system at  $998 \pm 10$  K. The overall error bars consist of three parts:  $\pm 10\%$  based on the accuracy of the photodiode,  $\pm 5\%$  considering the injection stability and a  $1\sigma$  error of the PIE curve averaged over the individual scans. The colored lines refer to the reference PIE curves of isomers and isotopes. The red lines show the overall fit via the linear combination of the reference curves.

Figure S5 exhibits PIE curves of  $m/z=123$ ,  $124$ ,  $125$ ,  $126$ ,  $127$  and Fig. S6 shows PIE curves of  $m/z=159$ ,  $160$ ,  $161$ ,  $162$ ,  $163$ ,  $164$ , which are related to two and one Cl atom(s) elimination from  $C_7H_5Cl_3$  molecule, respectively, in high experimental temperature. However, there is no corresponding reference data to have fits and identifications for species at these well-defined  $m/z$  ratio positions.

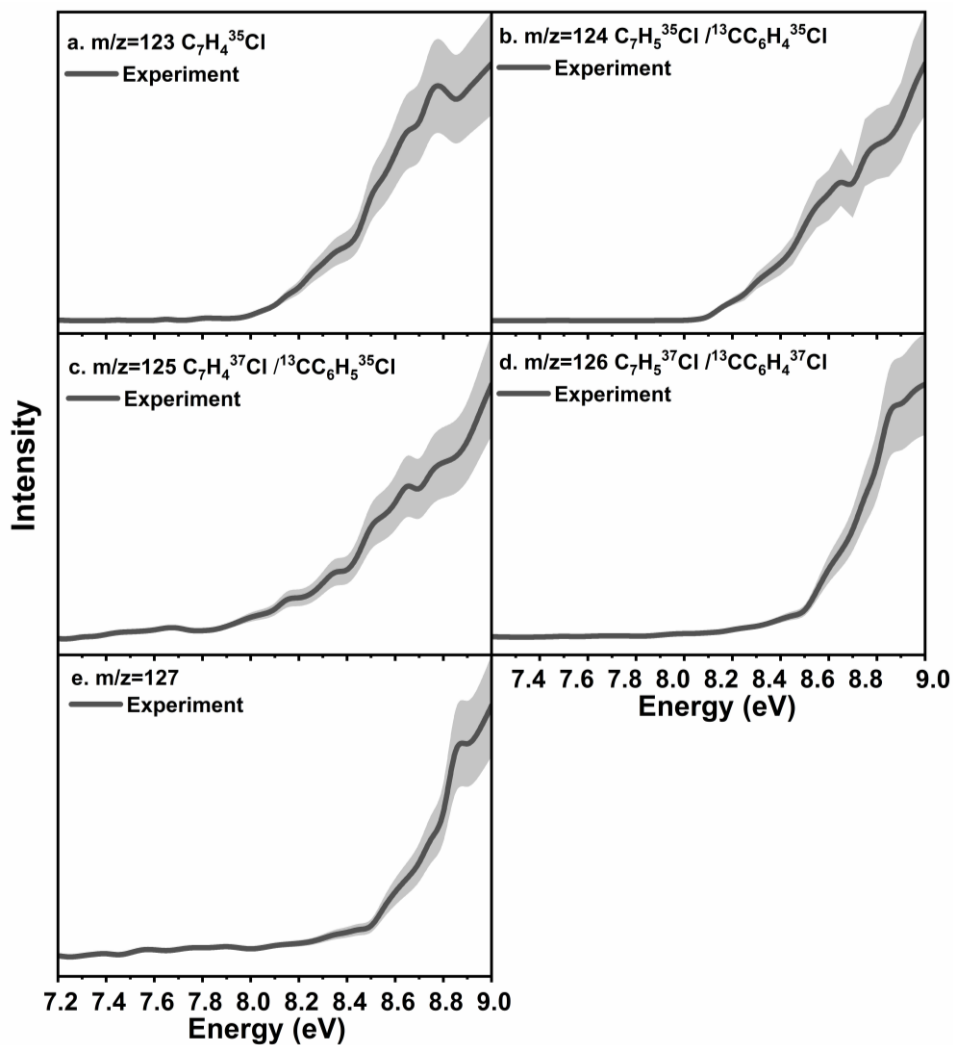


**Fig. S5** Experimental and reference PIE curves for species at  $m/z=123$ ,  $124$ ,  $125$ ,  $126$  and  $127$  in trichloromethyl-benzene ( $C_7H_5Cl_3$ ) /propargyl bromide ( $C_3H_3Br$ ) system at  $998 \pm 10$  K. The overall error bars consist of three parts:  $\pm 10\%$  based on the accuracy of the photodiode,  $\pm 5\%$  considering the injection stability and a  $1\sigma$  error of the PIE curve averaged over the individual scans.

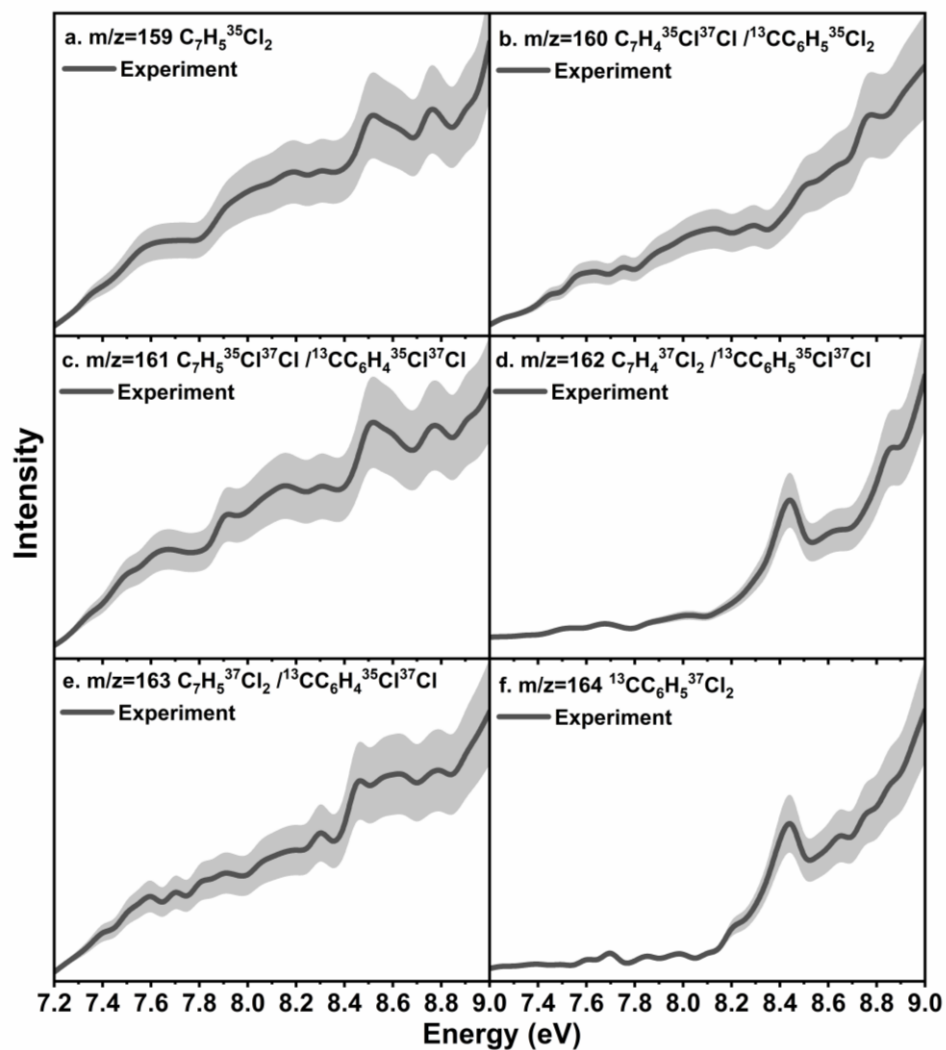


**Fig. S6** Experimental PIE curves for species at  $m/z=159$ ,  $160$ ,  $161$ ,  $162$ ,  $163$  and  $164$  in trichloromethyl-benzene ( $C_7H_5Cl_3$ )/propargyl bromide ( $C_3H_3Br$ ) system at  $998 \pm 10$  K. The overall error bars consist of three parts:  $\pm 10\%$  based on the accuracy of the photodiode,  $\pm 5\%$  considering the injection stability and a  $1\sigma$  error of the PIE curve averaged over the individual scans.

Ion counts for  $m/z=124$  ( $C_7H_5^{35}Cl^+$ ) and  $126$  ( $C_7H_5^{37}Cl^+$ ) result from two Cl atoms losing from  $C_7H_5Cl_3$  molecule in the elevated temperature. The integral value of ion count at  $m/z=126$  is about 33% of that at  $m/z=124$  in  $C_7H_5Cl_3/He$  system at 998 K, while this value rises to 102% in  $C_7H_5Cl_3/C_3H_3Br$  reactive system under the same experimental temperature. In order to

inspect the discrepancy, PIE curves of  $m/z=126$  in referred and reactive experiments are compiled in Fig. S7. It can be seen that tendencies of two PIE curves at  $m/z=126$  in both systems stay consistent before photon energy of 8.50 eV, whereas the obvious rising trend emerges at 8.50-9.00 eV for PIE curve in  $C_7H_5Cl_3/C_3H_3Br$  reactive system, which implies that the novel species with  $IE=8.50$  eV is generated at  $m/z=126$  in  $C_7H_5Cl_3/C_3H_3Br$  reactive system.

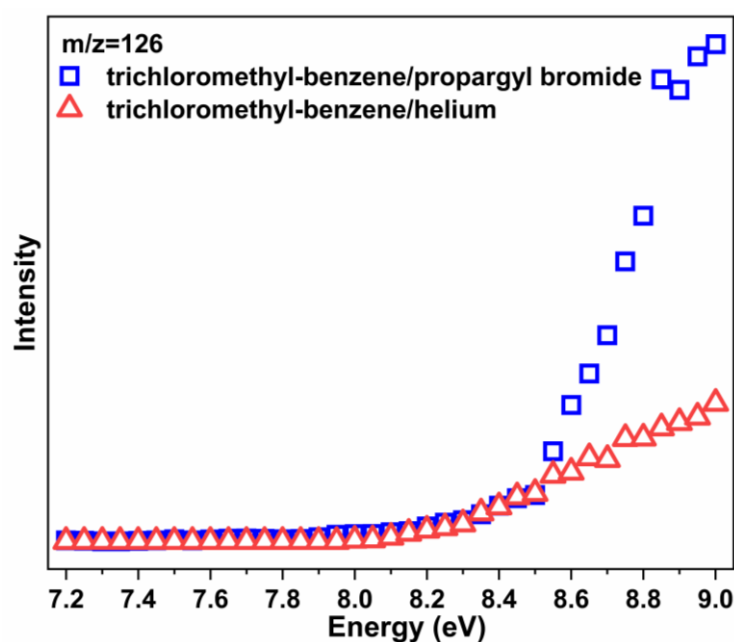


**Fig. S7** Experimental PIE curves for species at  $m/z=126$  at  $998 \pm 10$  K.

Experimental PIE curves for species at  $m/z=39$ , 78, 174, 176 and 178 in  $C_7H_5Cl_3/C_3H_3Br$  system at  $998 \pm 10$  K are given in Fig. S8. Propargyl ( $C_3H_3^*$ ) generated from the decomposition of  $C_3H_3Br$  can be identified without other species based on PIE curve of  $m/z=39$ . Byproducts, fulvene ( $C_6H_6$ ) and phenanthrene ( $C_{14}H_{10}$ ), are also detected and determined on the basis of experimental PIE curves of  $m/z=78$  and 178, which formed through self-recombination reactions of  $C_3H_3^*$  and  $C_7H_5^*$  radicals, respectively. Species at  $m/z=174$  and 176 could be generated from the H-elimination of products at  $m/z=178$ , but further identification cannot be made due to the lack of corresponding reference data.

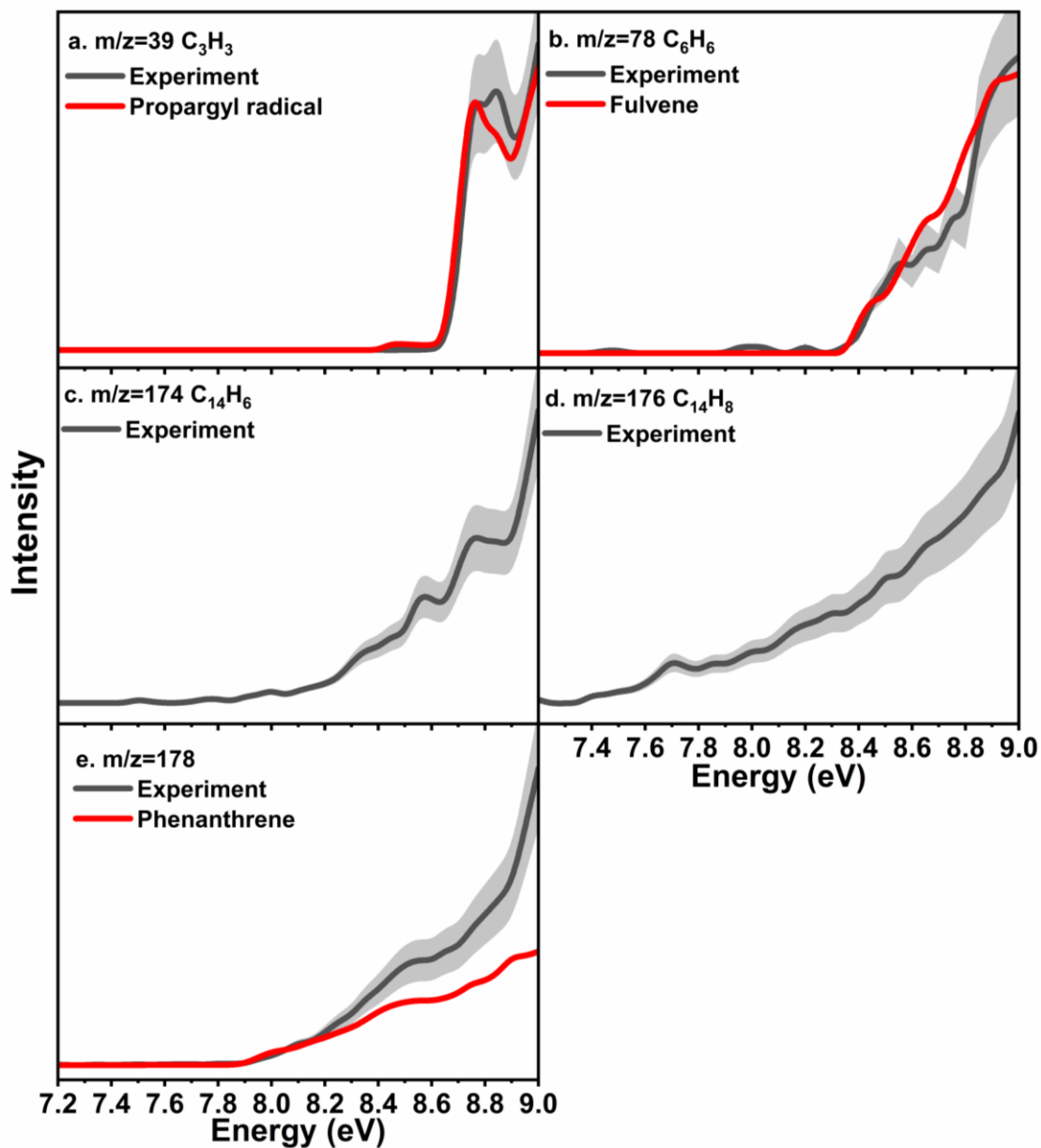


**Fig. S8** Experimental PIE curves for species at  $m/z=39$ , 78, 174, 176 and 178 in trichloromethyl-benzene ( $C_7H_5Cl_3$ )/propargyl bromide ( $C_3H_3Br$ ) system at  $998 \pm 10$  K. The overall error bars consist of three parts:  $\pm 10\%$  based on the accuracy of the photodiode,  $\pm 5\%$  considering the injection stability and a  $1\sigma$  error of the PIE curve averaged over the individual scans. The red lines refer to the reference PIE curves.

### Section 3: Phthalide pyrolysis.

Phthalide ( $C_8H_6O_2$ , Fig. S3a) has been employed as a precursor to generate fulvenallenyl through thermo-decomposition and the only product, fulvenallenyl, was detected and identified.<sup>7-9</sup> In order to verify the feasibility and efficiency of fulvenallenyl generation through trichloromethyl-benzene ( $C_7H_5Cl_3$ , Fig. S3b) pyrolysis at elevated temperature, the experiment of phthalide decomposition was also performed, using the facility as shown in Fig. S2, at Combustion Endstation (BL03U) of the National Synchrotron Radiation Laboratory (NSRL) in Hefei, China. Briefly, phthalide ( $C_8H_6O_2$ , 98%, Sigma-Aldrich) was prepared in the filter (Swagelok, SS-6F-MM-) and heated to 378 K by a heating tape. The helium gas (He, > 99.999%, 10.00 ml/min) entered the filter and carried the gas phthalide into the high-temperature reactor. The pressure of the gas mixture was maintained at 250 Torr; the micro reactor was heated to  $1073 \pm 10$  K. Under the above experimental condition, mass spectra of phthalide pyrolysis at 9.50 and 10.00 eV was acquired (Fig. S9) and the previous study has given the analysis for various ion counts in the spectra.<sup>8</sup> Meanwhile, the PIE curve of  $m/z=89$  (fulvenallenyl) in phthalide pyrolysis, from 8.00-9.00 eV in a step of 0.05 eV, was also collected (Fig. S10a), along with precursor's PIE data at  $m/z=134$  (Fig. S10b). It must be emphasized that the fulvenallenyl generation efficiency from phthalide pyrolysis is lower at 1073 K (Fig. S9), even at higher temperature (1273 K).<sup>8</sup>

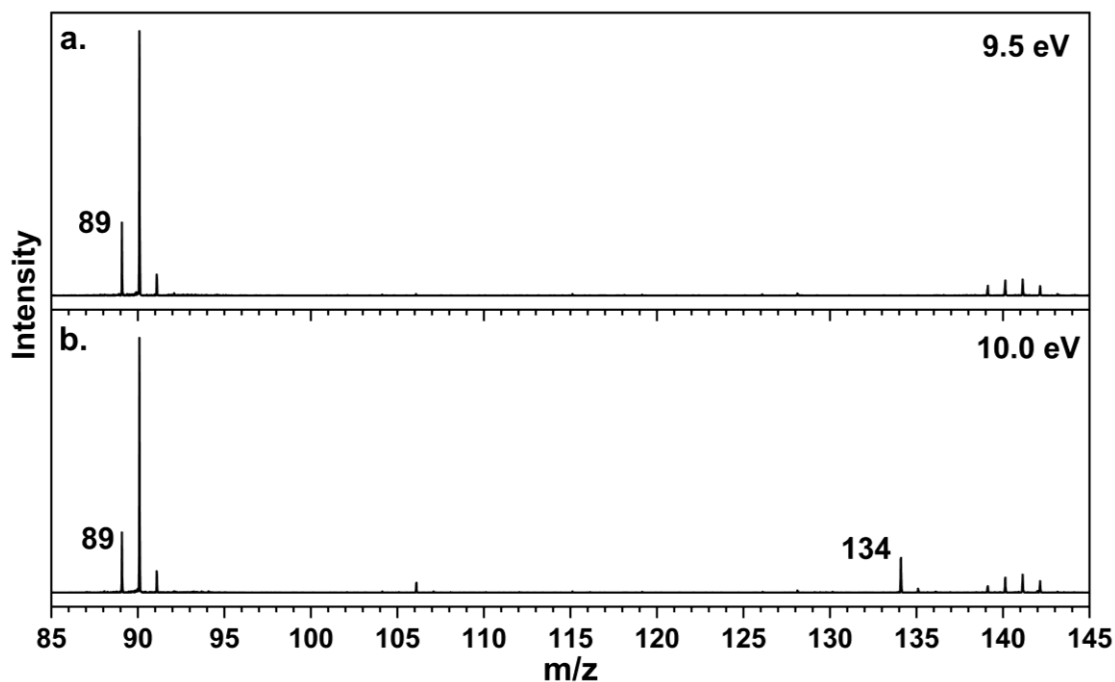


**Fig. S9** Mass spectra of phthalide pyrolysis at  $1073 \pm 10$  K recorded at the photoionization energy of (a) 9.50 eV and (b) 10.00 eV.

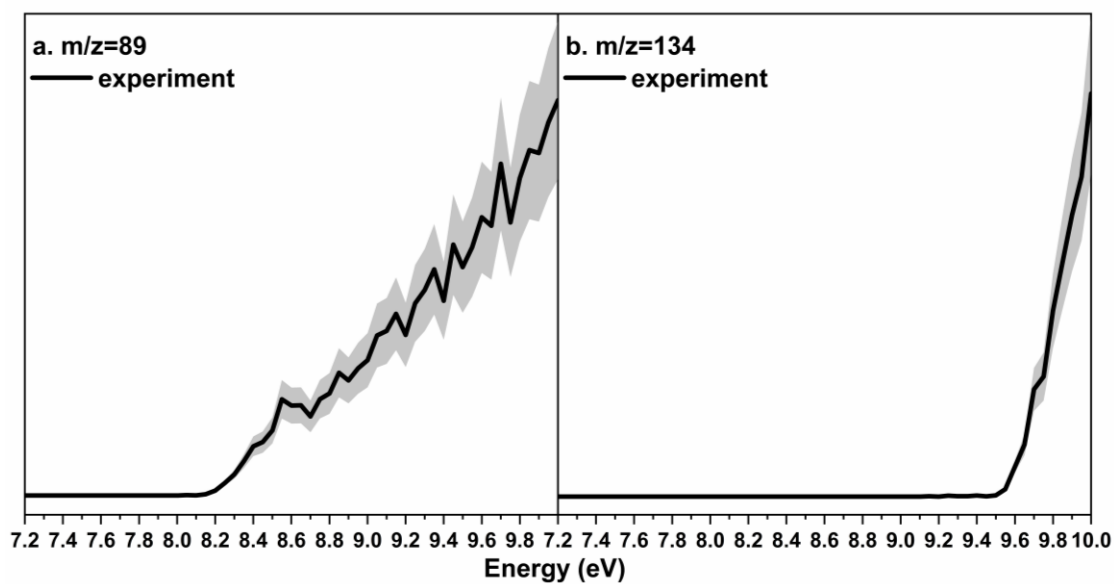


**Fig. S10** Experimental PIE curves for species at  $m/z = 89$  and  $134$  in phthalide pyrolysis system recorded at  $1073 \pm 10$  K.

Notably, except for phthalide, decomposition of toluene, at high temperature, proceeding by sequential loss of H atoms, can also generate fulvenallenyl.<sup>8,10</sup> The PIE data (Fig. S11a, red)

of fulvenallenyl from the toluene pyrolysis experiment,<sup>11</sup> using a long tube reactor, is also adopted to have a fit with the experimental PIE curve in trichloromethyl-benzene/propargyl bromide system and there is a great match (Fig. S11a). In addition, fulvenallenyl was also detected and identified in the high-temperature decomposition of JP-10 (exo-tetrahydrodicyclopentadiene)<sup>6</sup> and the corresponding PIE data was used to fit the experimental PIE curve in trichloromethyl-benzene/propargyl bromide system (Fig. S11b). Though the PIE curve from JP-10 pyrolysis shakes violently due to the low content of fulvenallenyl, the global tendency can match between two groups of PIE data. In conclusion, the current work provides convincing and powerful evidence on the generation of fulvenallenyl through trichloromethyl-benzene decomposition in the high temperature.

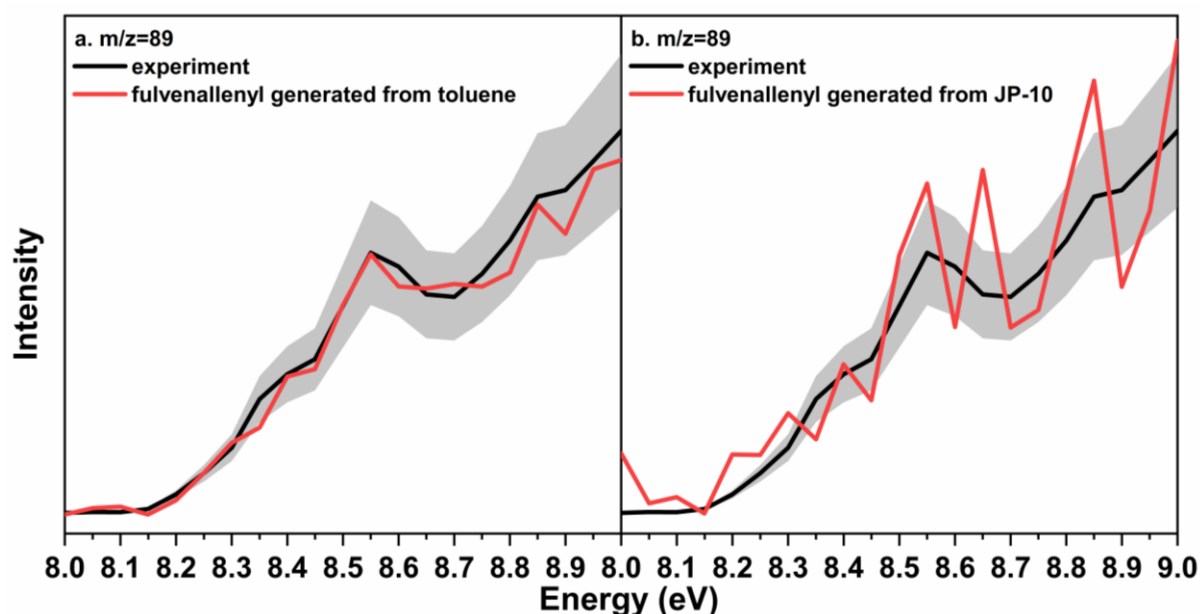


**Fig. S11** Experimental PIE (black) of  $m/z=89$  in trichloromethyl-benzene ( $C_7H_5Cl_3$ )/propargyl bromide ( $C_3H_3Br$ ) system. The red lines refer to PIE curves of fulvenallenyl, respectively generated from pyrolysis of (a) toluene and (b) JP-10.

#### Section 4: Absolute photoionization cross-section (PICS) of azulene.

To better identify and quantify the products, the measurement of absolute photoionization cross-section (PICS) of azulene ( $C_{10}H_8$ , Aladdin, > 97%) was also performed and the absolute PICS evaluation method adopted in this study has been detailly provided in the literature.<sup>12</sup> The brief description is given here.

For species  $i$ , the ion signal  $S_i$  can be written as:

$$S_i(E) = C \times X_i(E) \times \sigma_i(E) \times D_i \times \varphi_p(E)$$

Here  $C$  is a proportional constant;  $X_i(E)$  is the mole fraction of species  $i$  at photon energy  $E$ ;  $\sigma_i(E)$  is the photoionization cross-section of the species  $i$  at photon energy  $E$ ;  $D_i$  is the mass discrimination factor for species  $i$ ; and  $\varphi_p(E)$  is the photon flux. By taking benzene as the reference species, the PICS of species  $i$  can be calculated as:

$$\sigma_i = \sigma_{ref} \times \frac{X_{ref}(E)}{X_i(E)} \times \frac{S_i(E)}{S_{ref}(E)} \times \frac{D_{ref}}{D_i}$$

In the current work, benzene cross section was selected as calibration and reference curve ( $\sigma_{ref}$ ) in the azulene PICS measurement. The PICS of azulene was measured and determined using synchrotron vacuum ultraviolet photoionization (SVUV) and homemade reflection time-of-flight mass spectrometer (RTOF-MS)<sup>12</sup>. The solid azulene ( $C_{10}H_8$ , Aladdin, >97%, 0.2 g) was dissolved in liquid benzene ( $C_6H_6$ , Aladdin, >99.9%, 2.73 ml) and the mole fraction of azulene in mixture was calculated and controlled at 4.88%. The feeding rate (0.1 ml/h) of liquid mixture was controlled by the single channel syringe pump (LSP01–2A, Longer Precision Pump Co., Ltd) with a 5.00 ml syringe. The mixture was evaporated at 433 K in the vaporizer with the pressure of 780 Torr and the gas mixture was seeded in the carrier gas of argon (Ar, 300 ml/min). Gaseous mixture entered into a flow tube reactor (7.0 mm i.d., 10.0 mm o.d., 40.0 cm long,

made of corundum) at the temperature of 433 K and then was sampled forming the molecular beam through a quartz nozzle (0.35 mm diameter) and a Ni-skimmer (2.00 mm). The molecular beam entered into the synchrotron VUV photoionization chamber and sampled species was ionized by the tunable VUV light. Ions were collected and propelled into Re-TOF-MS in the photon energy range of 7.00 to 9.50 eV at a step-size of 0.05 eV. Figure S12a shows a cross-validation of the PICS evaluation method adopted in this study.<sup>12-14</sup> The experimental result of azulene PICS is provided in Fig. S12b and the onset value  $7.40 \pm 0.05$  eV can be determined.

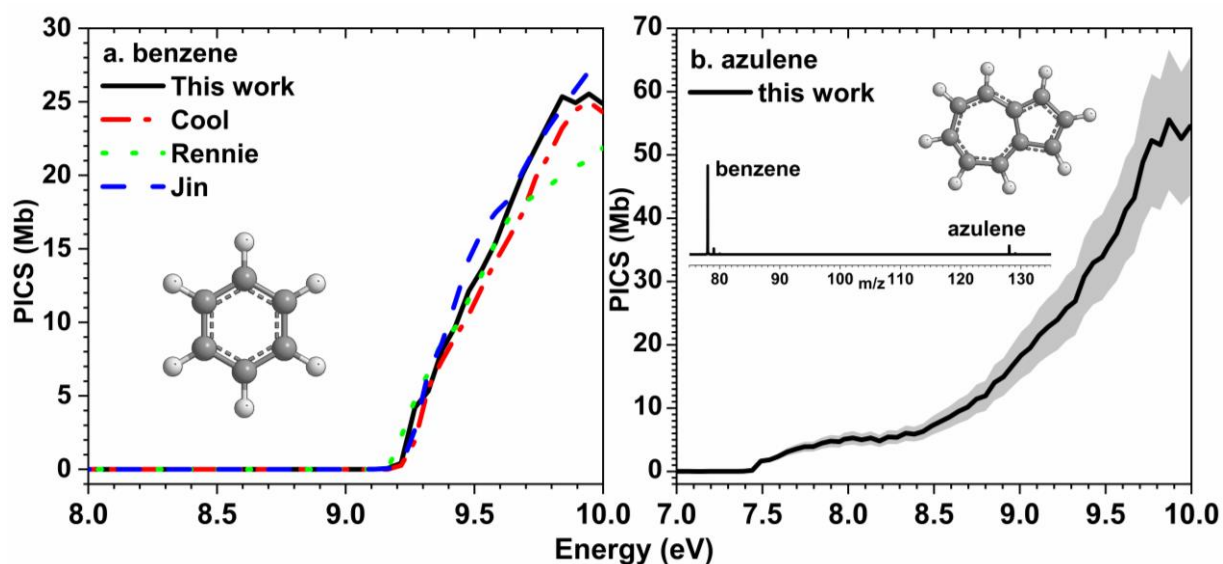


**Fig. S12** Experimental photoionization cross-section of azulene measured in Hefei.

## Section 5: Fit of PIE at $m/z = 128$ .

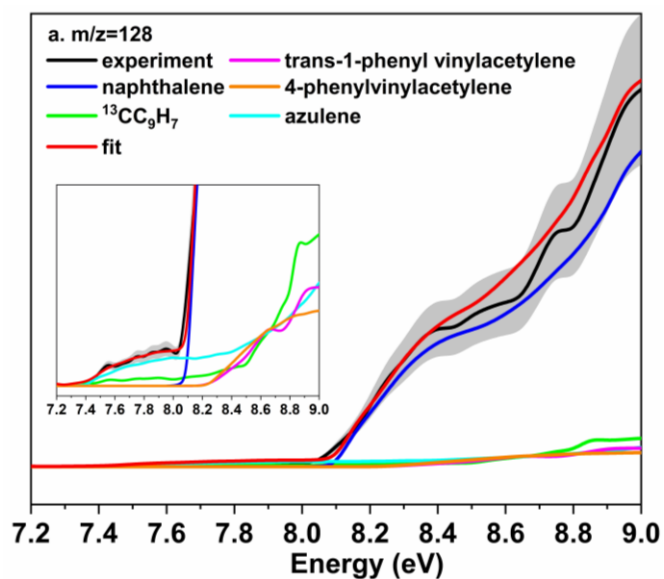


**Fig. S13** Experimental PIE curves for species at  $m/z = 128$  in the trichloromethyl-benzene ( $C_7H_5Cl_3$ )/propargyl bromide ( $C_3H_3Br$ ) system at  $998 \pm 10$  K, along with reference PIE data including 4-phenylvinylacetylene and *trans*-1-phenylvinylacetylene. It is clear that with the inclusion of the two  $C_{10}H_8$ , isomers 4-phenylvinylacetylene and *trans*-1-phenylvinylacetylene, the overall fit for  $m/z = 128$  could not match the experimental measurement.

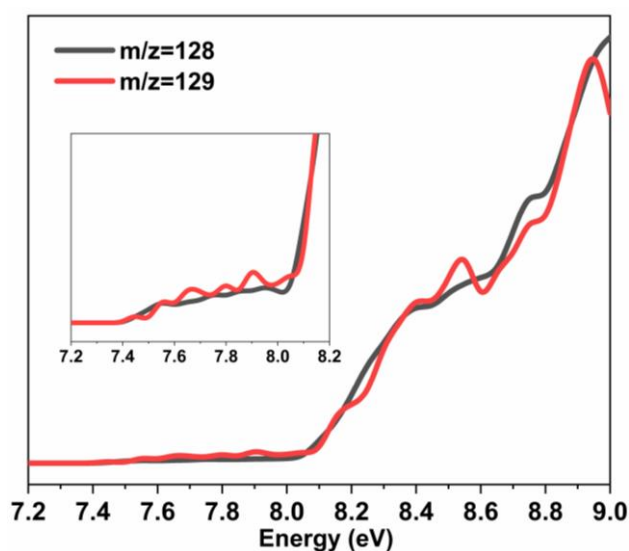


**Fig. S14** Comparison between the normalized experimental PIE curves for species at  $m/z = 128$  and 129 in the trichloromethyl-benzene ( $C_7H_5Cl_3$ )/propargyl bromide ( $C_3H_3Br$ ) system at  $998 \pm 10$  K.

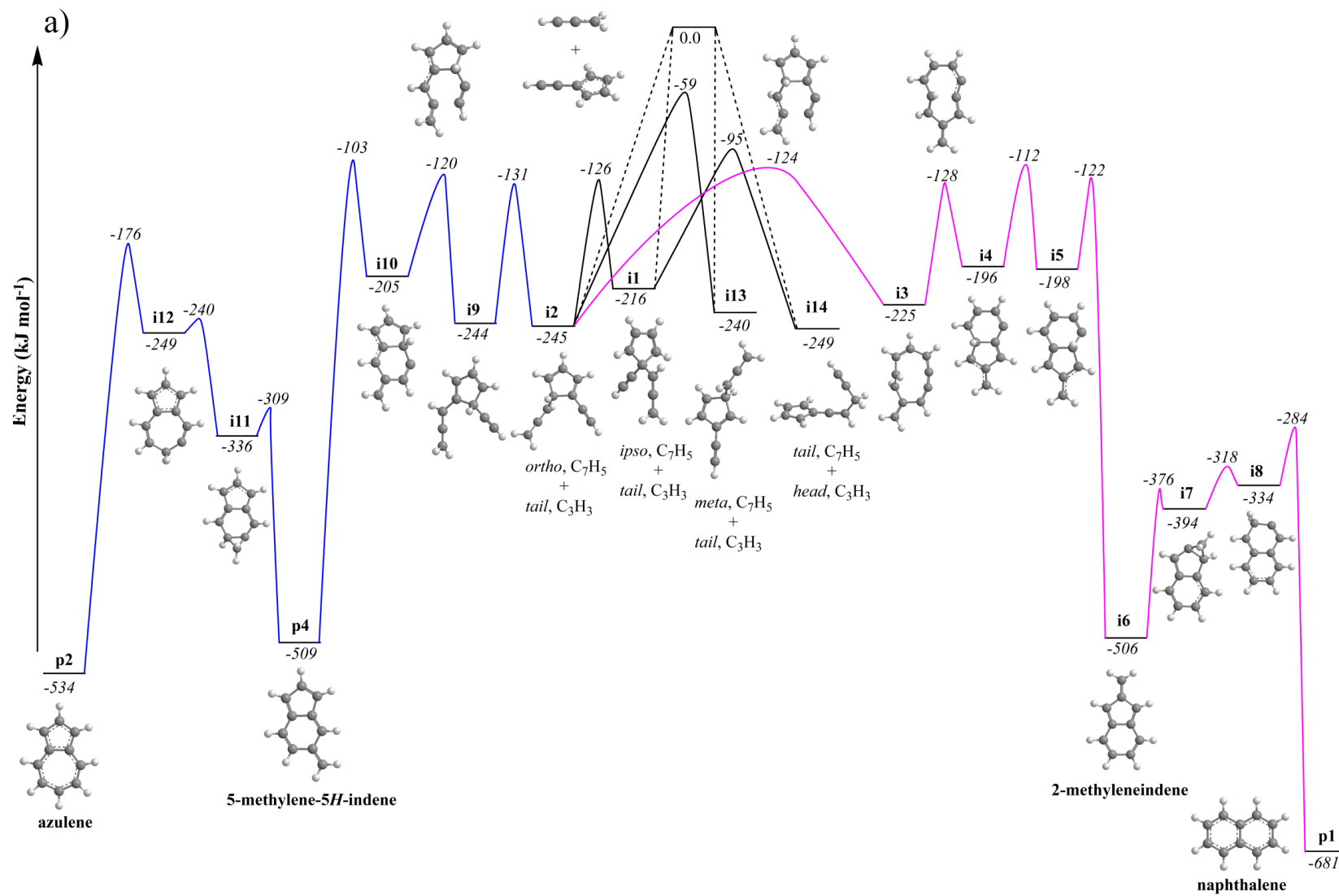
## Section 6: Computational methods.

Geometries of minima and transition states were optimized using the density functional theory (DFT) wB97XD<sup>15</sup> method with the 6-311G(d,p) basis set.<sup>16</sup> Vibrational frequencies and zero-point energies (ZPE) were computed at the same level of theory. All calculated minima have no imaginary frequencies and transition states have one imaginary frequency. All reaction pathways were verified by carrying out intrinsic reaction coordinate (IRC)<sup>17</sup> calculations at the wB97XD/6-311G(d,p) level of theory. The energies of the optimized minima and transition states with a closed-shell singlet character were refined using the explicitly correlated coupled clusters CCSD(T)-F12/cc-pVTZ-f12 method.<sup>18-20</sup> When T1 diagnostics of the stationary structures exceeded 0.02, indicating a multireference character of the wave function, the energies were calculated at the CASPT2(12e,12o)<sup>21,22</sup>/cc-pVTZ<sup>18</sup> level of theory. The T1 diagnostics is the norm of the vector of T1 amplitudes in the coupled cluster wave function scaled to be independent of the number of correlated electrons N. The (12e,12o) active space in the CASPT2 calculations included all  $\pi$  electrons and  $\sigma$  electrons involved in bond cleavage/formation or unpaired and the corresponding bonding and antibonding orbitals. Ionization energy of 5-methylene-5H-indene was computed through CBS-QB3 method based on the optimized structures at the B3LYP/6-311G(d,p) level of theory.<sup>23,24</sup> The DFT calculations were carried out using the Gaussian 16 program package,<sup>25</sup> whereas the coupled clusters, and CASPT2 calculations were performed using the MOLPRO 2010 program.<sup>26</sup>

Product branching ratios were computed using the Rice-Ramsperger-Kassel-Marcus (RRKM) Master Equation (ME) approach<sup>27</sup> as implemented in the MESS code.<sup>28</sup> Lennard-Jones ( $\epsilon/\text{cm}^{-1}$ ,  $\sigma/\text{\AA}$ ) = (390, 4.46) and the collisional energy transfer parameters  $n = 0.62$ ,  $\alpha_{300}$

= 424 cm<sup>-1</sup> used in the “exponential down” model<sup>29</sup> of the collisional energy transfer for the temperature dependence of the range parameter  $\alpha$  for the deactivating wing of the energy transfer function  $\alpha(T) = \alpha_{300}(T/300 \text{ K})^n$  were taken from the previous study of the C<sub>9</sub>H<sub>x</sub>/Ar systems.<sup>30</sup> The entrance reaction channels were treated within phase space theory<sup>31</sup> with equal rates constants from the formation of all eight entrance complexes. The branching ratios of the four prevailing products appear to be independent of the entrance branching between channels belonging to the same group and to depend only on the branching between the two groups, tail-to-tail plus head-to-ring vs. head-to-tail plus tail-to-ring.

## Section 7: Potential energy diagrams with representative transition state structures



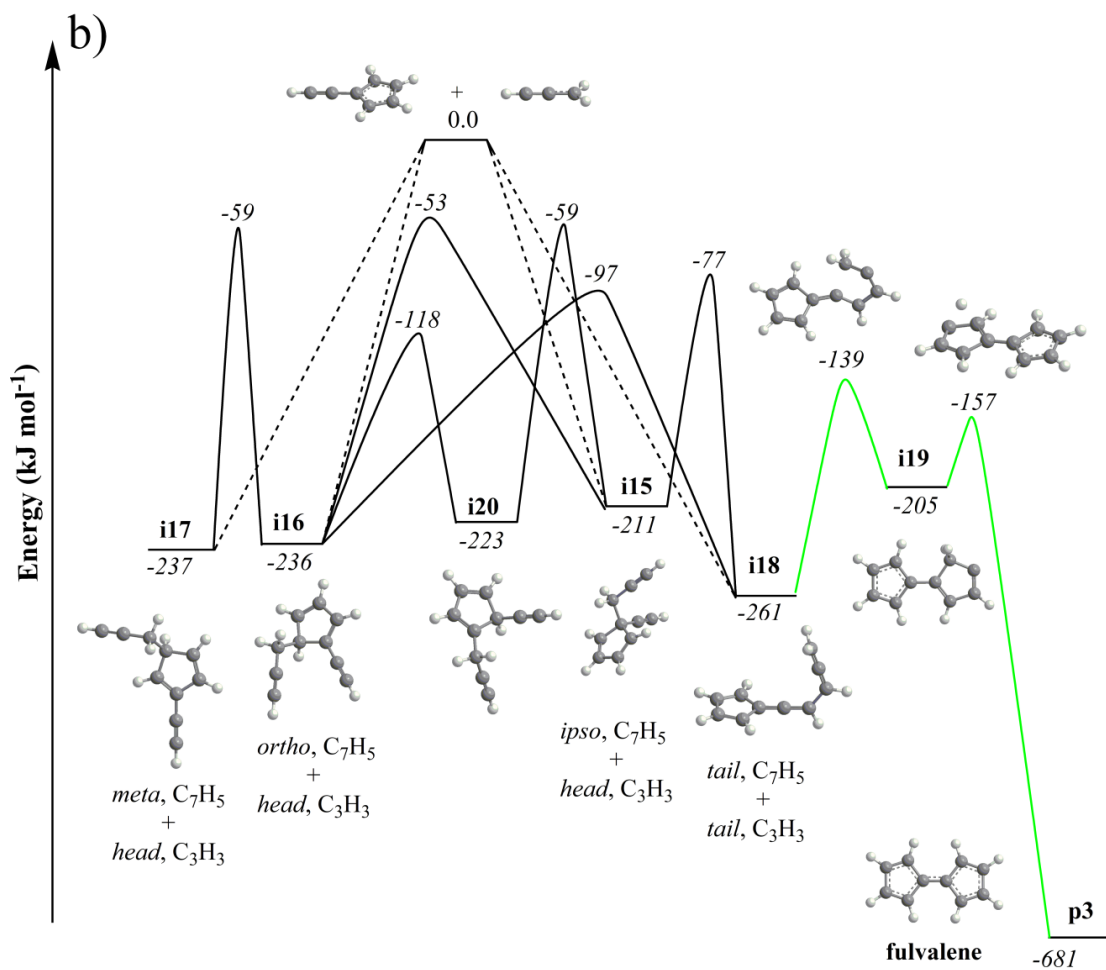


**Fig. S15** Most favorable reaction pathways of the reaction of fulvenallenyl (C<sub>7</sub>H<sub>5</sub><sup>\*</sup>) with propargyl (C<sub>3</sub>H<sub>3</sub><sup>\*</sup>) (a) to naphthalene and azulene and (b) to fulvalene illustrated with the structures of representative transition states.

## Section 8: Product branching ratios.

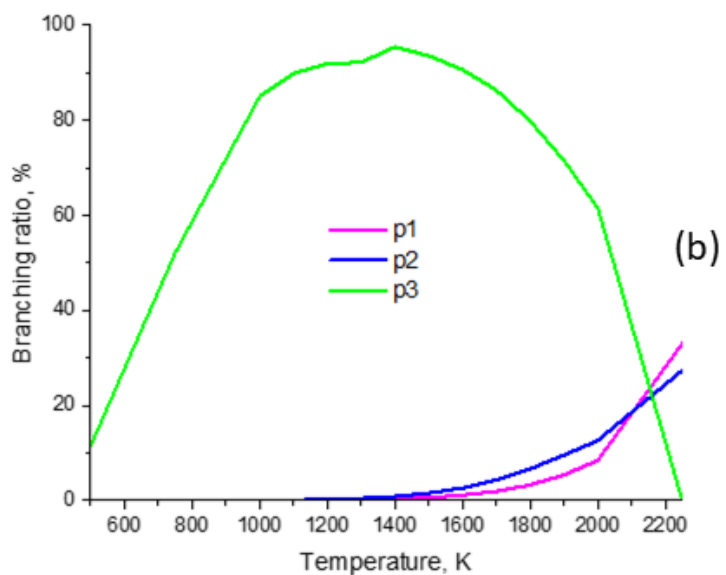
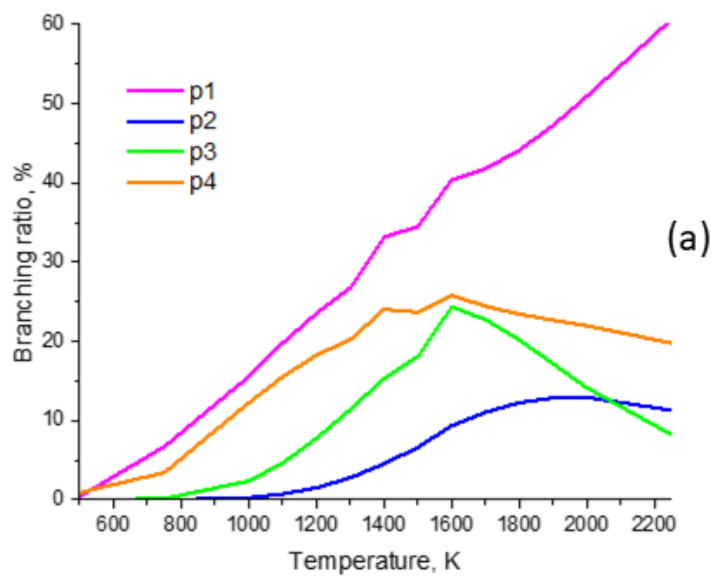


**Fig. S16** Product branching ratios computed at  $p = 0.01$  atm for two group of entrance channels, head-to-tail plus tail-to-ring group (a) and tail-to-tail plus head-to-ring (b).

## Reference.

1. D. E. Couch, A. J. Zhang, C. A. Taatjes and N. Hansen, Experimental observation of hydrocarbon growth by resonance stabilized radical-radical chain reaction, *Angew. Chem. Int. Ed.*, 2021, **60**, 27230-27235.
2. D. E. Couch, G. Kukkadapu, A. J. Zhang, A. W. Jasper, C. A. Taatjes and N. Hansen, The role of radical-radical chain-propagating pathways in the phenyl+propargyl reaction, *Proc. Combust. Inst.*, 2022, **39**, 643-651.
3. K. Moshhammer, L. Seidel, Y. Wang, H. Selim, S. M. Sarathy, F. Mauss and N. Hansen, Aromatic ring formation in opposed-flow diffusive 1,3-butadiene flames, *Proc. Combust. Inst.*, 2017, **36**, 947-955.
4. L. Ruwe, K. Moshhammer, N. Hansen and K. Kohse-Höinghaus, Influences of the molecular fuel structure on combustion reactions towards soot precursors in selected alkane and alkene flames, *Phys. Chem. Chem. Phys.*, 2018, **20**, 10780-10795.
5. Z. Zhou, X. Du, J. Yang, Y. Wang, C. Li, S. Wei, L. Du, Y. Li, F. Qi and Q. Wang, The vacuum ultraviolet beamline/endstations at NSRL dedicated to combustion research, *J. Synchrotron Radiat.*, 2016, **23**, 1035-1045.
6. L. Zhao, T. Yang, R. I. Kaiser, T. P. Troy, B. Xu, M. Ahmed, J. Alarcon, D. Belisario-Lara, A. M. Mebel, Y. Zhang, C. Cao and J. Zou, A vacuum ultraviolet photoionization study on high-temperature decomposition of JP-10 (exo-tetrahydrodicyclopentadiene), *Phys. Chem. Chem. Phys.*, 2017, **19**, 15780-15807.
7. C. Wentrup and P. Müller, One-step synthesis of fulvene and fulvenallene: Thermolysis of Q-coumaranon, phthalide, and benzocyclopropene, *Tetrahedron Lett.*, 1973, **14**, 2915-2918.
8. F. Hirsch, I. Fischer, S. Bakels and A. M. Rijs, Gas-phase infrared spectra of the C<sub>7</sub>H<sub>5</sub> radical and its bimolecular reaction products, *J. Phys. Chem. A*, 2022, **126**, 2532-2540.
9. M. Steinbauer, P. Hemberger, I. Fischer and A. Bodi, Photoionization of C<sub>7</sub>H<sub>6</sub> and C<sub>7</sub>H<sub>5</sub>: Observation of the fulvenallenyl radical, *Chemphyschem*, 2011, **12**, 1795-1797.
10. G. d. Silva, J. A. Cole and J. W. Bozzelli, Thermal decomposition of the benzyl radical to fulvenallene (C<sub>7</sub>H<sub>6</sub>)+H, *J. Phys. Chem. A* 2009, **113**, 6111-6120.
11. W. Yuan, Y. Li, P. Dagaut, J. Yang and F. Qi, Investigation on the pyrolysis and oxidation of toluene over a wide range conditions. I. Flow reactor pyrolysis and jet stirred reactor oxidation, *Combust. Flame*, 2015, **162**, 3-21.
12. H. Jin, J. Yang and A. Farooq, Determination of absolute photoionization cross-sections of some aromatic hydrocarbons, *Rapid Commun. Mass Spectrom.*, 2020, **34**, e8899.
13. E. E. Rennie, C. A. F. Johnson, J. E. Parker, D. M. P. Holland and M. A. Hayes, A photoabsorption, photodissociation and photoelectron spectroscopy study of C<sub>6</sub>H<sub>6</sub> and C<sub>6</sub>D<sub>6</sub>, *Chem. Phys.*, 1998, **229**, 107-123.
14. T. A. Cool, J. Wang, K. Nakajima, C. A. Taatjes and A. McLlroy, Photoionization cross sections for reaction intermediates in hydrocarbon combustion, *Int. J. Mass. Spectrom.*, 2005, **247**, 18-27.
15. J. D. Chai and M. Head-Gordon, Long-range corrected hybrid density functionals with damped atom-atom dispersion corrections, *Phys. Chem. Chem. Phys.*, 2008, **10**, 6615-6620.
16. P. C. Hariharan and J. A. Pople, The influence of polarization functions on molecular orbital hydrogenation energies, *Theoret. chim. Acta (Berl.)* 1973, **28**, 213-222.
17. H. P. Hratchian and H. B. Schlegel, Accurate reaction paths using a Hessian based predictor-

- corrector integrator, *J. Chem. Phys.*, 2004, **120**, 9918-9924.
18. T. Dunning, H. Jr., Gaussian basis sets for use in correlated molecular calculations. I. The atoms boron through neon and hydrogen, *J. Chem. Phys.*, 1989, **90**, 1007-1023.
  19. T. Adler, B., G. Knizia and H. J. Werner, A simple and efficient CCSD(T)-F12 approximation, *J. Chem. Phys.*, 2007, **127**, 221106.
  20. G. Knizia, T. B. Adler and H. J. Werner, Simplified CCSD(T)-F12 methods: Theory and benchmarks, *J. Chem. Phys.*, 2009, **130**, 054104.
  21. P. Celani and H. J. Werner, Multireference perturbation theory for large restricted and selected active space reference wave functions, *J. Chem. Phys.*, 2000, **112**, 5546-5557.
  22. T. Shiozaki, G. Werner, P. Celani and H. J. Werner, Communication: Extended multi-state complete active space second-order perturbation theory: Energy and nuclear gradients, *J. Chem. Phys.*, 2011, **135**, 081106.
  23. Z. S. Safi, N. Wazzan and H. Aqel, Calculation of vertical and adiabatic ionization potentials for some benzaldehydes using hybrid DFT, multilevel G3B3 and MP2 methods, *Chem. Phys. Lett*, 2022, **791**, 139349.
  24. A. F. Jalbout, A. M. Darwish and H. Y. Alkahby, Ionization energies, hardness, softness, and absolute electronegativity of heteronuclear and homonuclear diatomic molecules by the CBS-QB3 and G3B3 methods, *J. Mol. Struct.*, 2002, **585**, 205-208.
  25. M. J. T. Frisch, G. W.; Schlegel, H. B.; Scuseria, G. E.; Robb, M. A.; Cheeseman, J. R.; Scalmani, G.; Barone, V.; Petersson, G. A.; Nakatsuji, H.; Li, X.; Caricato, M.; Marenich, A. V.; Bloino, J.; Janesko, B. G.; Gomperts, R.; Mennucci, B.; Hratchian, H. P.; Ortiz, J. V.; Izmaylov, A. F.; Sonnenberg, J. L.; Williams-Young, D.; Ding, F.; Lipparini, F.; Egidi, F.; Goings, J.; Peng, B.; Petrone, A.; Henderson, T.; Ranasinghe, D.; Zakrzewski, V. G.; Gao, J.; Rega, N.; Zheng, G.; Liang, W.; Hada, M.; Ehara, M.; Toyota, K.; Fukuda, R.; Hasegawa, J.; Ishida, M.; Nakajima, T.; Honda, Y.; Kitao, O.; Nakai, H.; Vreven, T.; Throssell, K.; Montgomery, J. A., Jr.; Peralta, J. E.; Ogliaro, F.; Bearpark, M. J.; Heyd, J. J.; Brothers, E. N.; Kudin, K. N.; Staroverov, V. N.; Keith, T. A.; Kobayashi, R.; Normand, J.; Raghavachari, K.; Rendell, A. P.; Burant, J. C.; Iyengar, S. S.; Tomasi, J.; Cossi, M.; Millam, J. M.; Klene, M.; Adamo, C.; Cammi, R.; Ochterski, J. W.; Martin, R. L.; Morokuma, K.; Farkas, O.; Foresman, J. B.; Fox, D. J. Gaussian, Inc., Wallingford CT, 2016, Gaussian 16, Revision C.01. *Journal*, 2016.
  26. H. J. Werner, P. J. Knowles, G. Knizia, F. R. Manby and M. Schutz, Molpro: a general-purpose quantum chemistry program package, *WIREs Comput. Mol. Sci.*, 2012, **2**, 242-253.
  27. Y. Georgievskii, J. A. Miller, M. P. Burke and S. J. Klippenstein, Reformulation and solution of the master equation for multiple-well chemical reactions, *J. Phys. Chem. A*, 2013, **117**, 12146-12154.
  28. Y. Georgievskii and S. J. Klippenstein, MESS Program Package, <https://tcg.cse.anl.gov/papr/>, 2015.
  29. J. Troe, Theory of thermal unimolecular reactions at low pressures. I. Solutions of the master equation, *J. Chem. Phys.*, 1977, **66**, 4745-4757.
  30. A. M. Mebel, Y. Georgievskii, A. W. Jasper and S. J. Klippenstein, Pressure-dependent rate constants for PAH growth: Formation of indene and its conversion to naphthalene, *Faraday Discuss.*, 2016, **195**, 637-670.
  31. S. J. Klippenstein and J. I. Cline, Classical phase space theory for product state distributions

with application to the v-j vector correlation, *J. Chem. Phys.*, 1995, **103**, 5451-5460.